PaleoBios 26(2):27–36, October 13, 2006

Using paleosols of the Picture Gorge Basalt to reconstruct the middle Miocene climatic optimum

NATHAN D. SHELDON
Department of Geology, Royal Holloway University of London, Egham, Surrey TW20 OEX, United Kingdom;
n.sheldon@gl.rhul.ac.uk

The Picture Gorge Subgroup of the Columbia River Basalt preserves numerous, minimally altered, interflow paleosols that were formed during the middle Miocene climatic optimum. These paleosols are used to reconstruct a high-resolution paleoclimate record. Between 16.0–15.4 Ma ago, mean annual precipitation (MAP) was 500–900 mm/year and mean annual temperature (MAT) was 8–16°C, which is consistent with independent estimates of paleoprecipitation and paleotemperature from fossil plants and paleosols of the contemporaneous Mascall Formation. The record suggests cooling and aridification similar to marine foraminiferal isotopic records. One possible cause for the middle Miocene climatic optimum is transient elevated atmospheric CO_2 levels, though some recently compiled marine isotopic records indicate near-modern CO_2 levels. This possibility is explored using an equilibrium model to simulate the formation of the dominant Picture Gorge paleosol type. Model results indicate elevated CO_2 levels 2–3 times present atmospheric levels were necessary to form the observed mineral assemblage and mass-balance characteristics of the paleosols. This result is consistent with stomatal index studies of gingkos and laurels, which indicate CO_2 levels 2–4 times present atmospheric levels.

INTRODUCTION

Recent compilations of Phanerozoic atmospheric pCO_2 based on the stomatal index of plants (Retallack 2001a; Kuerschner et al. 2002), and foraminiferal boron isotopes (Pearson and Palmer 2000; Demicco et al. 2003) indicate transient greenhouse conditions in the middle Miocene. This short-lived warming event, named the middle Miocene climatic optimum, is indicated independently by paleosols, marine foraminifera and molluscs of Japan (Itoigawa and Yamanoi 1990), South Australia (McGowran and Li 1997), and Germany (Schwarz 1997). Additional evidence comes from fossil plants (Utescher et al. 2000), and $\delta^{13}C$ and $\delta^{18}O$ isotopes from benthic foraminifera (Zachos et al. 2001). Western U.S. floras at 49 Camp, Fingerrock, Pyramid, Mascall, and Latah indicate an unusually warm and wet paleoclimate at 16 Ma, but much drier and cooler conditions by 15 Ma (Graham 1999). Middle Miocene (at ~16 Ma) fossil floras of North America had high percentages of exotic plants from Asia (Graham 1999), which is the likely source of elephants, gelocid deer, and other mammal immigrants to North America at the same time (Janis et al. 1998). Similarly, in Oregon marine rocks, larger foraminifera and corals occur in the Astoria Formation for only a restricted interval centered around 16 Ma, whereas other parts of the formation have less diverse molluscan faunas (Moore 1963), and cool climate indicators such as glendonites (ikaite pseudomorphs; Boggs 1972).

It has been suggested recently that CO_2 and climate may have been decoupled for some climatic events (Cowling 1999). For example, Royer et al. (2001) failed to find significantly elevated pCO_2 for the interval of the middle Miocene climatic optimum based on paleobotanical data straddling the event temporally. Carbon isotopic proxies based on pedogenic carbonate (Ekart et al. 1999; Tanner et al. 2001) and on marine phytoplankton compared with foraminifera (Pagani et al. 1999, 2000) also appear to indicate a CO_2-temperature decoupling. The pCO_2 levels calculated by Pagani et al. (2000) and Royer et al. (2001) are below modern pre-Industrial levels. Retallack (2001a, 2002) suggested that isotopic proxies may be compromised by methane clathrate dissociation events, which release extremely isotopically light carbon. Furthermore, new stomatal index data, located temporally during the transient event instead of flanking it (as in Royer et al.'s 2001 data), indicate elevated atmospheric pCO_2 levels during the middle Miocene climatic optimum (Kuerschner et al. 2002; Retallack 2002). The purpose of this study is to address whether the observed degree of weathering among middle Miocene paleosols could have occurred under near-modern pCO_2 levels, or whether elevated pCO_2 levels were necessary to account for the observed weathering.

An ideal data set to examine the middle Miocene climatic optimum event at high resolution is the Picture Gorge Subgroup of the Columbia River Basalt Province (Figure 1). The

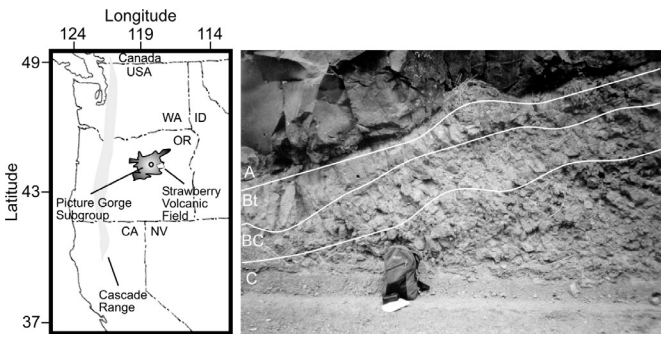

Figure 1. Location map and field photo. The photo is of a typical Ilukas paleosol and the overlying basalt flow.

Picture Gorge Subgroup has preserved numerous interflow paleosols of varying degrees of development. The Picture Gorge Subgroup was emplaced at ~16.5–15.6 Ma (Baksi 1989), and its stratigraphic relationships have been well established (Bailey 1989). The middle Miocene climatic optimum has been dated to ~16 Ma as well (Hornibrook 1990; Zachos et al. 2001). Five paleosol pedotypes have been identified as having formed in ecosystems ranging from swamps (peaty soils) to forests (Sheldon 2003), and they are placed within the overall Cenozoic paleoenvironmental context of the John Day Basin (Retallack, personal comm.).

Sheldon (2003) reconstructed Picture Gorge paleoenvironmental conditions on the basis of physical characteristics and geochemistry of the paleosols, and performed a number of mass-balance calculations to show losses and gains of various elements as a result of pedogenesis. Although it is possible to reconstruct paleoprecipitation and paleotemperature estimates on the basis of bulk rock geochemistry (see below; Sheldon et al. 2002), it is difficult to reconstruct the paleoatmospheric pCO_2 that contributed to those paleoclimatic conditions in paleosols that lack pedogenic carbonate.

This paper will present two new findings: (1) a high-resolution paleoclimatic record for the interval from 16.1–15.4 Ma ago, and (2) results of an attempt to use an equilibrium weathering model to assess atmospheric pCO_2 ~16 Ma ago.

PALEOSOLS OF PICTURE GORGE

Sheldon (2003) identified five different types of paleosols in Picture Gorge, two of which preserve direct fossil evidence of previous ecosystems. Cenozoic paleosols of central Oregon are organized into pedotypes (similar to soil series) and given names in the local Sahaptin language (Retallack et al. 2000). Three of the five types of paleosols preserved in Picture Gorge are too poorly developed to be used for quantitative paleoclimatic or paleoenvironmental analysis, and also do not preserve plant or animal fossils (Sheldon 2003). In contrast, the two more well-developed Ilukas and Monana types of paleosols preserve plant and animal fossils.

Ilukas (*firewood*) paleosols, which preserve rare terrestrial gastropods but no plant fossils, are the most common type of paleosols preserved in the Picture Gorge Subgroup of the Columbia River Basalt (Figure 1), and are described in detail elsewhere (Sheldon 2003). To summarize, the Ilukas paleosols are typically very red (5YR4/4 to 10R4/4) with A-Bt-BC-C profiles, and are similar to well-aerated Alfisols (Tables 1 and 2; Sheldon 2003). The Monana (*around underneath*) pedotype is black and brown (2.5Y5/2) with O/A-A2-A3-C profiles (Tables 1 and 2), and was probably once a poorly aerated, histic Inceptisol (Sheldon 2003). The Monana pedotype does not preserve any animal fossils, but plant fossils are common throughout the A, A2, and A3 horizons.

The difference in fossil preservation between Ilukas (gastropods, no plants) and Monana (no animals, plants) paleosols is likely due to soil aeration and alkalinity/acidity in the soils during their formation. Well-aerated, alkaline soils

Table 1. Paleoclimatically significant Picture Gorge pedotypes.

Pedotype	Diagnosis	FAO[a]	USDA[b]
Monana *underneath*[1]	granular structure clayey peat over grey-green volcanisclastic sandstone parented by basalt	Humic Cambisol	Humaquept
Ilukas *firewood*	thick and red with clayey subsurface (Bt) horizons parented by basalt	Luvisol	Udalf

[1]Italicized text is the translation of the pedotype name from Sahaptin into English.
[a]FAO (1988)
[b]Soil Survey Staff (1975)

Table 2. Paleoenvironmental interpretation of interflow paleosols.

Pedotype	Paleoclimate	Former Vegetation	Paleotopography	Parent Material	Time
Monana	subhumid, seasonally dry	peat swamp, seasonally dry	boggy floodplain depression	volcaniclastic sandstones and	500–5000
Ilukas	humid (600–1200 mm/yr), seasonally dry	upland old growth eutrophic forest, seasonally dry	flow top topography, well-drained	tholeiitic basalt	20000–75000

preserve bones and shells, but plants are oxidized and decay readily, whereas poorly aerated, acid soils dissolve bones and shells but readily preserve plants (Retallack 2001b).

HEATING BY THE OVERRIDING BASALT FLOW

Although much of the organic matter in Picture Gorge Subgroup paleosols was lost to post-burial processes, the histic epipedon of the Monana pedotype preserved an amount sufficient for vitrinite reflectance analysis. Samples collected from within 3 cm of the contact with the overlying flow have a mean reflectance value of 1.14 (medium volatile bituminous coal), declining 6 cm below the contact to a mean reflectance of 0.80 (high volatile bituminous coal). At 10 cm below the contact, the mean reflectance is just 0.32 (lignite-grade), which is consistent with normal diagenesis rather than any significant heating of the paleosol by the overlying basalt flow. All of the samples have a small population of higher reflectance values representing degrado-fusinite, which is formed by fungi oxidizing humic kerogen. This process increases the carbon content, and thus the hardness and reflectance of the organic matter. Thus, only vitrinite was used to determine the maturity of the samples, and those results suggest heating to 160–180°C within the upper 6 cm of the Monana profile, but declining to no more than 60–80°C at a depth of 10 cm (Mukhopadhyay 1992).

Comparison between thin sections prepared from the basalt-paleosol contact and thin sections of red, smectitic clays fired into pottery shows significant petrographical differences. Paleosol samples exhibit high birefringent clays and show typical soil fabrics, whereas the pottery samples lack birefringence and have an amorphous clay fabric consistent with the heating they experienced (Sheldon 2003). Furthermore, the distribution of alkali elements within the paleosols is consistent with pedogenic processes, including cycling of airborne additions from nearby silicic volcanism, rather than with metasomatic alteration due to basalt flow emplacement (Sheldon 2003). These results, combined with the quantitative heating estimates derived from the vitrinite reflectance analyses, indicate that the paleosols were minimally altered by heating associated with the emplacement of the basalt flows (Sheldon 2003).

PALEOCLIMATIC RECONSTRUCTION

Picture Gorge preserves a number of paleosols that can be used to reconstruct a high-resolution paleoclimatic record. As discussed in the previous section, the original chemistry of the paleosols seems to have been robustly preserved (Sheldon 2003). Sheldon et al. (2002) demonstrated that the chemical composition of paleosol Bt and Bw horizons may be applied to reconstruct mean annual precipitation (MAP) and mean annual temperature (MAT) using empirical relationships derived from modern soils. MAP may be calculated with reasonable precision and accuracy ($R^2 = 0.72$; $p < .0001$) as:

$$\text{MAP (mm)} = 221.1e^{.0197(CIA\text{-}K)} \quad (1)$$

where CIA-K is the molar ratio of Al_2O_3 to Al_2O_3, CaO, and Na_2O multiplied by 100 (Maynard 1992). MAT may be calculated with much less precision but similar accuracy ($R^2 = 0.37$; $p < .0001$) as:

$$\text{MAT (°C)} = -18.5S + 17.3 \quad (2)$$

where S is the molar ratio of K_2O and Na_2O to Al_2O_3. Using this approach to reconstruct Eocene and Oligocene paleoclimatic conditions gave estimates of both MAT and MAP that corresponded well with estimates derived from independent paleoclimatic proxies including paleosol Bk horizon depth and plant fossils (Sheldon et al. 2002).

A final consideration in making a paleoclimatic reconstruction is an age model. Based on the total number of mapped basalt flows in the Picture Gorge Subgroup and the total duration of their emplacement, the average time represented by each basalt flow is 8300 years (e.g., Tolan et al. 1989). Soil Bt horizon thickness can be related to formation time using modern soil data (from Markewich et al. 1990) to develop the following empirical relationship:

$$\text{Age (years)} = 17.07\,(\textit{Bt thickness}) + 645.8\,(\textit{Bt thickness}) \quad (3)$$

with $R^2 = 0.87$. No correction for compaction (e.g., Sheldon and Retallack 2001) is necessary because these paleosols were never deeply buried and because the basalt in the sequence is effectively un-compactible. By counting the number of basalt flows between paleosols and using equation (3) to calculate the duration of soil formation, it is possible to assign an approximate age to each of the paleosols in the succession (Table 3) starting from the Skaw paleosol, which was dated at 16.0 ± 0.2 Ma (C. Swisher 1995 unpublished data).

Figure 2 depicts the reconstructed paleoclimatic conditions (MAP and MAT) obtained from equations (1) and (2) (original geochemical data available from the author) plotted against paleosol ages determined using equation (3). The reconstructed MAP of 500–900 mm/yr and MAT of 8–16°C represent temperate, sub-humid conditions consistent with independent estimates of MAP and MAT from fossil plants and paleosols elsewhere in Oregon (Retallack et al. 2000). There is some suggestion that cooling and drying occurred from 16–15.5 Ma ago, but there are too many uncertainties in the estimates to be any more precise. However, global climatic conditions cooled and aridified significantly by ~15 Ma (e.g., Graham 1999; Zachos et al. 2001), thus suggesting that the trend observed in these data may be real.

EQUILIBRIUM MODELING

Soils are excellent recorders of environmental conditions because they form in direct contact with the atmosphere. As a result, gas contents in soils equilibrate with atmospheric gases. However, soil respiration, especially in tropical settings, may lead to soil pCO_2 that is 100–200 times higher than that of the atmosphere (Brook et al. 1983; Volk 1987). Thus, the minimum soil pCO_2 expected is the atmospheric pCO_2. Elevated soil pCO_2 values are associated with high-

biomass systems or with waterlogged settings where diffusive loss of soil pCO_2 to the atmosphere (if soil pCO_2 > atmospheric pCO_2) is inhibited. Thus, a well-drained soil with low to moderate productivity will generally have soil $pCO_2 \approx$ atmospheric pCO_2. Weathering reactions can be most tightly constrained when the chemical composition of the protolith is well understood. The Ilukas pedotype paleosols of Sheldon (2003) formed *in situ* on basalt flow tops. However, not all of the Picture Gorge paleosols fulfill these criteria. The Monana pedotype also formed *in situ* on basalt, but it is a histic Inceptisol (peaty, moderately developed soil) that shows evidence of gleying. Because it formed in waterlogged conditions, it is likely that there was incomplete exchange of gases between the soil and the atmosphere. The Skaw and Kwalk pedotypes (Sheldon 2003) formed on reworked volcanic ash, so it is difficult to differentiate weathering related only to pedogenesis from the weathering associated with the redeposition of the ash. Thus, only the Ilukas and Nuqwas pedotypes fulfill the criteria of being well-drained, of having low to moderate productivity, and of forming *in situ* on basalt, and Ilukas paleosols are much more common than Nuqwas paleosols.

Because the atmospheric pCO_2 level is unlikely to have been lower than the soil pCO_2 levels, equilibrium modeling of abiotic weathering reactions can constrain minimum atmospheric pCO_2 levels. In other words, if present levels of pCO_2 are sufficient to create the observed degree of weathering in these paleosols, then it is likely that paleo-atmospheric pCO_2 levels were also at near-modern levels because biota can only serve to enhance the degree of weathering. This approach is somewhat indirect, but the thermodynamics of microbial and plant interactions during weathering are still poorly understood.

The computer program CHILLER (e.g., see Palandri and Reed 2001) allows users to calculate heterogeneous equilibrium of gas-mineral-water systems. CHILLER forces equilibrium with different gas mixes by treating gases as homogeneous minerals. In other words, a water-rock system in equilibrium with present atmospheric conditions is in equilibrium with the "minerals" called fCO2-3.5 (CO_2 fugacity = $10^{-3.5}$) and fO2-0.7 (O_2 fugacity = $10^{-0.7}$). New CO_2 "minerals" were created for 0.1, 1, 3, 5, 10, 15, and 20 times present atmospheric levels (PAL) assuming a present day atmospheric pCO_2 of $10^{-3.5}$ (for dilute mixtures, e.g., CO_2 in the atmosphere, $f \approx p$). All equilibrium K values are from the SOLTHERM database (construction of the database is outlined in Palandri and Reed 2001). The basic equation that controls the availability of CO_2 is:

$$H_2O_{(aq)} + CO_{2\,(g)} = HCO_3^-{}_{(aq)} + H^+{}_{(aq)}. \quad (4)$$

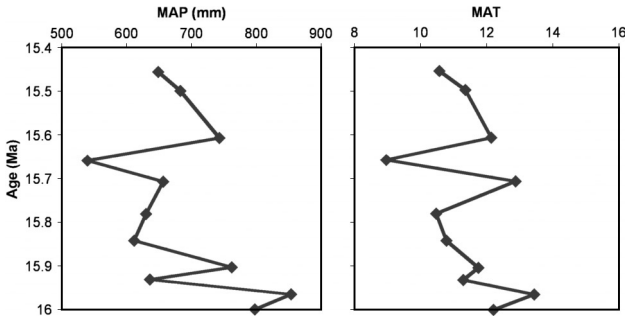

Figure 2. Reconstructed MAP and MAT. The standard error of the MAP estimates is ±182 mm/yr, and the standard error of the MAT estimates is ±4°C. Data for the ~15.9 Ma paleosol is from Sheldon (2003); all of the other estimates in Table 3 are based on newly collected data.

Table 3. Paleoclimatic data.

Pedotype	Age (Ma)	Bt thick (cm)	Time (yrs.)	MAP (mm)	MAT (°C)
Skaw	16.000	n.a.	n.a.		
Monana	15.965	n.a.	500–5000	854 (1)	13.4 (1)
Ilukas	15.932	20	19744	636 (2)[1]	11.3 (2)
Ilukas	15.904	40	53144	762 (1)	11.8 (1)
Ilukas	15.842	40	53144	612 (1)	10.8 (1)
Ilukas	15.781	46	65827	630 (2)	10.5 (2)
Ilukas	15.707	33	39900	657 (2)	12.9 (2)
Ilukas	15.659	35	43514	540 (2)	8.97 (2)
Ilukas	15.607	90	100000	743 (2)	12.1 (2)
Ilukas	15.499	30	34737	683 (1)	11.4 (1)
Ilukas	15.455	50	74965	649 (2)	10.6 (2)

[1]Number of individual chemical analyses averaged to obtain the paleoclimatic estimate.

From here, a K value may be calculated from the following (where a is activity):

$$K = \frac{a_{HCO_3^-} a_{H^+}}{f_{CO_2} a_{H_2O}} \quad (5)$$

Rearranging that expression (equation 6) and taking the Log_{10} of both sides (equation 7) allows us to calculated a new K value (here called K*) that can be used to force equilibrium with a given atmospheric CO_2 value.

$$(f_{CO_2})K = \frac{a_{HCO_3^-} a_{H^+}}{a_{H_2O}} \quad (6)$$

$$\text{Log}\, K^* = \text{Log}(f_{CO_2}) + \text{Log}\, K = \text{Log}\frac{a_{HCO_3^-} a_{H^+}}{a_{H_2O}} \quad (7)$$

For example, to create a new CO_2 gas "mineral" that corresponds to present-day atmospheric conditions (i.e., $pCO_2 = 10^{-3.5}$ bars), the following expression would be used:

$$\text{Log}\ K^* = 10^{-7.818} + 10^{-3.5}. \quad (8)$$

O_2 fugacity was kept constant at present levels, which is reasonable because oxygen levels are thought to have been roughly constant throughout the Cenozoic. CHILLER is set up to compute different water-rock ratios by "titrating" rock into a water (Figure 3) and recording how that water changes composition in response to the addition of rock. If precipitation is approximately constant through time, then there should be a systematic decrease in the amount of water that reacted with the parental basalt with increasing depth in the profile (Figure 3). Thus, by graphing results depicting ascending water-rock ratios from the top down, an artificial soil profile may be modeled. These artificial profiles obtained for equilibrium with different CO_2 levels (0.1-20 PAL) can then be compared with actual geochemical data on mass balance and the mineral assemblage from Sheldon (2003).

Table 4 summarizes the input parameters used in this modeling. Because rainwater is very fresh (i.e., has low salinity and low total-dissolved solids), most of the cations available for reactions come from the rock(s) being weathered. Pedogenesis is dominated by the breakdown of base-bearing minerals either by hydrolysis (e.g., potassium feldspar being weathered to illite) or by acid attack that liberates cations for use by plants and microbes. An example of the latter type of reaction would be the dissolution of albite as:

$$NaAlSi_3O_{8\ \text{albite}} + 4H^+ = Na^+ + Al^{3+} + 3SiO_2 + 2H_2O \quad (9)$$

where most of the resulting species are aqueous. Acid attack reactions consume H^+ ions, thereby raising the pH of

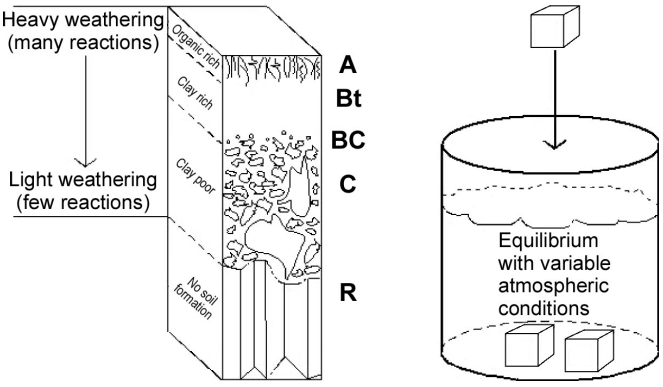

Figure 3. Cartoon depicting the equilibrium model.

Table 4. Input parameters for equilibrium modeling.

Rainwater Composition (mg/l)[b]				Basalt Composition (weight %)[c]			
pH[a]	5.47	HCO_3^-	152	SiO_2	50.7	MgO	5.00
Cl^-	3.47	$SiO_{2\ (aq)}$	8.6	TiO_2	1.55	CaO	9.83
SO_4^{2-}	2.19	Fe^{TOT}	0.05	Al_2O_3	15.1	Na_2O	2.91
Ca^{2+}	1.52	HPO_4^-	0.1	FeO	5.79	K_2O	0.74
Mg^{2+}	0.39	$O_{2\ (aq)}$	0.1	Fe_2O_3	5.71	P_2O_5	0.22
K^+	0.35	Al^{3+}	0.1	MnO	0.18	LOI	2.06
Na^+	2.05	Mn^{2+}	0.1				
NO_3^-	0.24						

[a] $pH = -Log_{10}(aH^+)$

[b] Rainwater composition #2 in the SOLTHERM database augmented by groundwater composition #5. The last four values (0.1) are not based on analytical results, but were used as input parameters because CHILLER requires input values for cations and anions that are to be speciated.

[c] This basalt analysis is from Sheldon (2003) and is typical of Picture Gorge Subgroup lavas. All of the loss on ignition was treated as H_2O gas. Because the thermodynamic properties of titanium species in solution are poorly understood, titanium was not included in the equilibrium calculations. This simplification is justified as titanium is extremely refractory during weathering, and is often taken to be an immobile element (e.g., Chadwick et al. 1990).

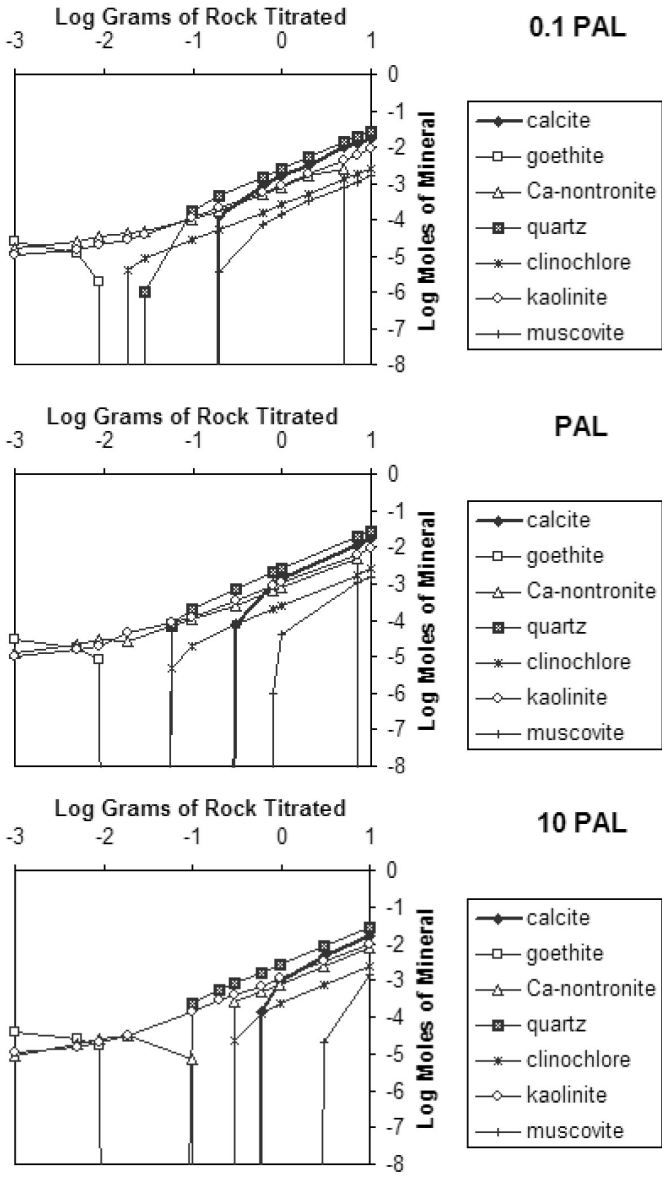

Figure 4. Minerals precipitated as a function of reaction extent. Calcite and muscovite form progressively later in the reaction with increasing pCO_2 level. In all three cases, the mineral assemblage at the first precipitation of calcite is quartz, kaolinite, Ca-nontronite, and clinochlore with minor amounts of daphnite, Mn-clinochlore, and MnO_2.

the system. While HCO_3^- is the most stable carbon-bearing species at near neutral pH values (6–8), CO_3^{2-} becomes the most stable species at higher pH values (>8). This change leads to the precipitation of carbonate minerals such as calcite, siderite, and ankerite. However, all of the interflow paleosols of the Picture Gorge Subgroup are carbonate-free, so the first appearance of carbonate minerals can be taken to represent the end point of the realistic weathering reaction.

Atmospheric pCO_2 values of 0.1, 1, 3, 5, 10, 15, and 20 PAL were used in model calculations, where 0.1 PAL is an extreme case used to represent the sub-modern pCO_2 levels suggested by Pagani et al. (2000) and Royer et al. (2001). All model calculations were for 25°C temperature conditions. While this reaction temperature may be slightly higher than the temperature at which the Picture Gorge Subgroup paleosols formed, it is no more than 10°C high (Figure 2), and is probably very close based on paleobotanical estimates (Graham, 1999). Using a reaction temperature of 25°C has the additional advantage of being the temperature at which most thermodynamic data are best-constrained. All model calculations were run over the range of 0.001–10 grams of rock added to a kilogram of water, or 10^{-3} to 10^{1} grams of rock titrated. In all cases, calcite precipitated before the end of the titration run. Taking into account both kinetic factors and the temperature, a number of zeolite and high-temperature minerals were suppressed from forming in the calculations.

MODEL RESULTS

Using the first appearance of calcite as the upper limit to the extent of the weathering reactions (i.e., the maximum amount of rock that can be titrated), more rock can be titrated into solution if the system is at higher pCO_2 conditions. At 0.1 PAL (an unrealistically low pCO_2 value), just 0.099 to 0.199 grams of rock were titrated before calcite precipitation occurred. At 10 PAL, 0.599 grams of rock were titrated before calcite precipitation, or 3–6 times more rock than the 0.1 PAL case and 2 times more rock than the 1 PAL case (Figure 4). Regardless of the pCO_2 used, a substantial quantity of goethite (FeOOH or $Fe(OH)_3$) forms at very high water-rock ratios and is replaced by minor amounts of daphnite ($Fe_5Al_2Si_3O_{10}(OH)_8$). In all of the runs, quartz is thermodynamically favored and precipitates as the dominant mineral phase in the final mineral assemblage. However, quartz precipitation is extremely slow, especially at 25°C, so most of the silica would actually be in amorphous colloidal phases in a typical soil. The assemblage in all of the runs of quartz, kaolinite, Ca-nontronite, and clinochlore with minor amounts of daphnite, Mn-clinochlore, and MnO_2 at the time of calcite precipitation is a good approximation of the actual mineral assemblage reported by Sheldon (2003). Clinochlore is a good proxy for metastable Mg-smectite (e.g., Mg-nontronite) minerals that typically form in soils formed under non-tropical precipitation regimes (Retallack 2001b). For example, in the 10 PAL case, Mg-nontronite precipitates and persists briefly before it is replaced by clinochlore.

It is possible to quantify the loss of a given element relative to its protolith composition using mass-balance calculations that assume an immobile element (Brimhall and Dietrich, 1987; Brimhall et al. 1991; Chadwick et al. 1990; Chadwick et al. 1999). Sheldon (2003) showed that Zr is nearly immobile and can be used to quantify the translocations of a number of weatherable cations. In addition to equation 9 above, equations 10-11 demonstrate the type of dissolution reactions common during the weathering of basalt:

$$Mg_2SiO_{4\ \text{forsterite}} + 4H^+ = 2Mg^{2+} + SiO_{2\ (aq)} + 2H_2O \qquad (10)$$

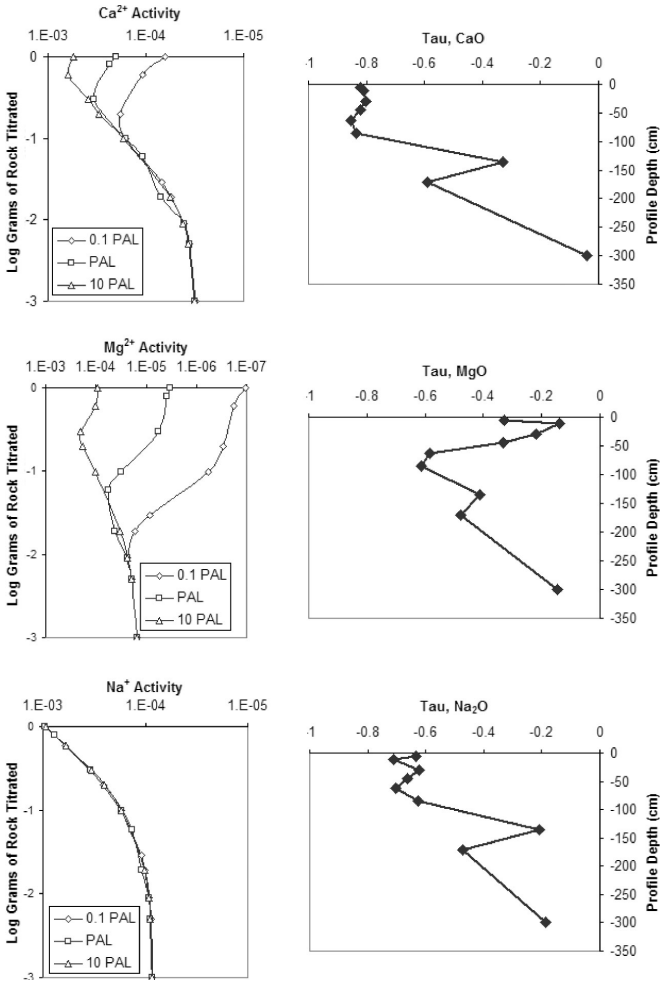

Figure 5. Losses of weatherable cations and modeled activities of weatherable cations. The left column contains the model results and the right column the measured weathering (translocations) from Sheldon (2003). A tau value of 0 corresponds to no change in a cation relative to the protolith, where a tau value of –1.0 corresponds to 100% loss of a cation. The slight decreases in some of the cations near the "surface" of the model soils are due to the precipitation of calcite, which briefly upsets the weathering process.

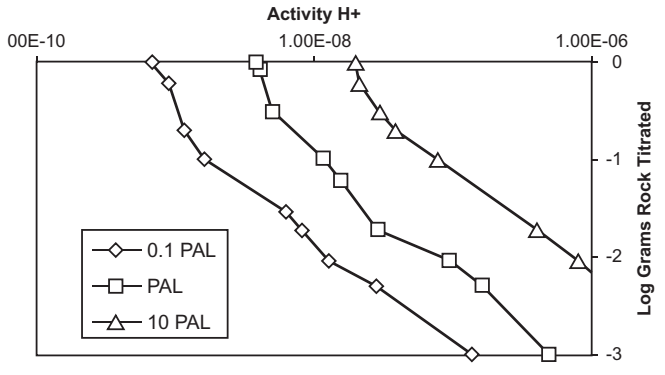

Figure 6. Changes in pH for model runs. The negative log of the activity of hydrogen is the pH, so higher activities of hydrogen correspond to lower pH values.

$$CaAl_2Si_2O_{8\ anorthite} + 8H^+ = Ca^{2+} + 2Al^{3+} + 2SiO_{2\ (aq)} + 4H_2O \quad (11)$$

Figure 5 shows the losses (negative translocations) of Ca^{2+}, Na^+, and Mg^{2+} from reactions 9–11 as a function of depth within the paleosol profile compared to the model calculations. Weathering is typically most intense near the surface of a soil and declines rapidly with increasing depth and decreasing permeability (both initial and as a direct result of plant-rock interactions). Therefore, with the titration of progressively more rock into solution we would expect an increase in the activity (and by extension, molality) of a given cation. This pattern is observed in the model calculations for the cations most germane to pedogenesis (i.e., the bases K^+, Na^+, Ca^{2+}, and Mg^{2+}), as shown in Figure 5.

DISCUSSION AND CONCLUSIONS

While increasing pCO_2 does not affect the liberation of Na^+ (Figure 5), there are roughly three orders of magnitude difference in Mg^{2+} (Figure 5) between the 0.1 PAL and 10 PAL model calculations, and nearly two orders of magnitude difference between the 1 PAL and 10 PAL. In the actual translocations calculated for Picture Gorge paleosols, as much as 80% of the original Ca^{2+} and 70% of the original Na^+ are lost, while only about 30% of the original Mg^{2+} was lost from the soil profile (Sheldon 2003). The Mg^{2+} that was displaced from the weathering of olivine and various pyroxenes was largely retained in the profile within Mg-smectites. While all three model cases precipitate clinochlore (our proxy for Mg-smectite), only the 10 PAL case liberates enough Mg^{2+} to account for the Mg-rich paleosol profiles that are observed, and it is also the only case to reproduce the "shape" of the data. Further, in higher pCO_2 model calculations (i.e., 20 PAL), dolomite precipitates, and dolomite is both kinetically and thermodynamically unlikely to form in soils except for unusual cases (Capo et al. 2000).

Figure 6 depicts the changes in pH in each of the model runs. At 0.1 PAL the pH at the top of the model soil profile is 9.2, at PAL it is 8.4, and at 10 PAL it is 7.7. Alfisols typically have pH values between 6.0 and 8.5, therefore the 1 PAL and 10 PAL cases fall within the range of realistic values for Alfisols (i.e., Ilukas pedotype). At pH > 8.0 chert commonly forms *in situ* in soils (Retallack 2001b). Sheldon (2003) did not find chert in any of the Picture Gorge Subgroup paleosols. In addition, carbonate minerals are most stable at higher pH values (Retallack 2001b), and the Picture Gorge Subgroup paleosols are carbonate-free, thereby suggesting near-neutral pH values during their formation, again most consistent with the 10 PAL. It is possible that carbonate minerals formed in the Picture Gorge Subgroup paleosols could have dissolved out and that it would have been better to consider the reaction between 1 and 10 grams of rock titrated rather than between 0.1 and 1 grams of rock titrated. This objection can be addressed by considering the water-rock ratios at which carbonate minerals began to form. The climatic transfer function based on the degree of chemical

weathering (equation 1; Sheldon (2003), gives a MAP of 748 ± 182 mm (standard error, rather than standard deviation) for the type Ilukas paleosol, and comparable estimates for the other Ilukas paleosols (Table 3). The formation time of most of the Ilukas paleosols is ~20,000–75,000 years based on comparison to modern soils and measurement of the Bt horizon thickness (Table 3; Sheldon 2003). For 1 m^3 of basalt ($\rho = 2.7$ g cm^{-3}) and the MAP and formation time above, a first-order calculation yields a range of water-rock ratios of ~5500 to 20,780. At 0.199 g of rock titrated (the first precipitation of calcite in the 0.1 PAL case), the water-rock ratio is 5115. For the PAL and 10 PAL model runs, the water-rock ratios are within a factor of three of the range of water-rock ratios obtained from the estimation based on MAP. This suggests that using the model results up through 1 gram of rock added is a good approximation for the real water-rock ratio that the Picture Gorge Subgroup paleosols experienced.

The 10 PAL model run is favored for three reasons. First, only the 10 PAL case produces a significant amount of Mg^{2+}. This value is an upper limit though, because higher pCO_2 values result in dolomite precipitation and dolomite is not observed in the paleosols and is unlikely to form in any soils for kinetic reasons (Capo et al. 2000). Second, pH values produced by the 10 PAL case are near neutral, consistent with the lack of soil carbonate and chert, and within the typical range associated with Alfisols, the soil type being modeled. Third, the 10 PAL case produces water-rock ratios that are close to those predicted by a simple calculation using the MAP and formation time estimates of Sheldon (2003).

That the 10 PAL case best matches the geologic evidence raises the question of how much of that total pCO_2 is due to atmospheric pCO_2 and how much is due to soil productivity. Using the world soil pCO_2 map of Brook et al. (1983), modern soils like the Picture Gorge Subgroup paleosols have 3–8 PAL soil pCO_2. Assuming that 10 PAL is the total pCO_2, from both atmospheric and soil respiration sources, necessary to produce the Picture Gorge Subgroup paleosols, atmospheric pCO_2 likely ranged from 2–7 PAL for the transient middle Miocene climatic optimum. Even at the low end of that range, it is clear that sub-pre-Industrial atmospheric pCO_2 levels, as suggested by Pagani et al. (1999, 2000), are too low. A value of 2–4 PAL is consistent with estimates from stomatal index (Kuerschner et al. 2002; Retallack 2002) and mass-balance modeling (Berner and Kothavala 2001). While this value would not represent a "super greenhouse" like that of the Jurassic and Cretaceous, it would still be a significant enhancement above the near-modern levels that persisted throughout much of the Cenozoic (Berner and Kothavala 2001). Given the extensive evidence for a transient warming event, it is unlikely that atmospheric CO_2 was decoupled from climate during the middle Miocene climatic optimum. The failure of isotopic proxies to detect elevated CO_2 levels may be due the influx of isotopically light carbon from methane release, as previously suggested by Retallack (2001a, 2002).

These model results do not preclude the possibility of very low atmospheric pCO_2 coupled with non-analogous biotic productivity in the Ilukas paleosols. However, the flora and fauna of the middle Miocene was not substantially different than modern in terms of community structure and ecology, so it is likely that modern-analogue forests have comparable productivity to their Miocene counterparts. Therefore, these results are suggestive that the middle Miocene warm event was due, at least in part, to elevated atmospheric pCO_2.

CONCLUSIONS

1) Paleosols preserved between basalt flows of the Picture Gorge Subgroup of the Columbia River Basalt province are well-preserved and can be used to reconstruct paleoclimatic conditions.

2) New geochemical results from paleosol Bt horizons indicate declining MAP and MAT between 16–15.4 Ma ago, consistent with global cooling observed in a number of independent terrestrial and marine proxies.

3) Equilibrium modeling of the atmospheric pCO_2 levels necessary to result in the observed soil formation indicates values 2–4 times present atmospheric levels. While there are a number of assumptions in the model regarding solution chemistry and biotic productivity levels, the results are consistent with previous pCO_2 estimates from mass-balance modeling and from the stomatal index of plant fossils.

ACKNOWLEDGEMENTS

This work was funded by NSF Grant EAR000953, and by a student research grant from the Penn State Astrobiology Research Center. This paper benefited from thoughtful reviews by Dennis Terry and Steve Driese.

LITERATURE CITED

Bailey, M.M. 1989. Revisions to the stratigraphic nomenclature of the Picture Gorge Basalt Subgroup, Columbia River Basalt Group. Pp. 67-84 *in* S.P. Reidel and P.R. Hooper (eds.). Volcanism and Tectonism in the Columbia River Flood-Basalt Province. *Geological Society of America Special Paper* 239.

Baksi, A.K. 1989. Reevalution of the timing and duration of extrusion of the Imnaha, Picture Gorge, and Grande Ronde Basalts, Columbia River Basalt Group. Pp. 105–111 *in* S.P. Reidel and P.R. Hooper (eds.). Volcanism and Tectonism in the Columbia River Flood-Basalt Province. *Geological Society of America Special Paper* 239.

Berner, R.A., and X. Kothavala. 2001. GEOCARBIII: a revised model of atmospheric CO_2 over Phanerozoic time. *American Journal of Science* 301:182–204.

Boggs, S. 1972. Petrography and geochemistry of rhombis, calcite pesudomorphs from mid-Tertiary mudstones. *Sedimentology* 19: 219–235.

Brimhall, G.H., and W.E. Dietrich. 1987. Constitutive mass balance relations between chemical composition, volume, density, porosity, and strain in metasomatic hydrochemical systems: results on weathering and pedogenesis. *Geochimica et Cosmochimica Acta* 51:567–587.

Brimhall, G.H., C.J. Lewis, C. Ford, J. Bratt, G. Taylor, and O. Warin. 1991. Quantitative geochemical approach to pedogenesis: importance of parent material reduction, volumetric expansion, and eolian influx in laterization. *Geoderma* 51:51–91.

Brook, G.A., M.E. Folkoff, and E.O. Box. 1983. A world model of soil carbon dioxide. *Earth Surface Processes and Landforms* 8:79–88.

Capo, R.C., C.E. Whipkey, J.R. Blachere, and O.A. Chadwick. 2000. Pedogenic origin of dolomite in a basaltic weathering profile, Kohala peninsula, Hawaii. *Geology* 28:271–274.

Chadwick, O.A., G.H. Brimhall, and D.M. Hendricks. 1990. From a black to a gray box—a mass balance interpretation of pedogenesis. *Geomorphology* 3:369–390.

Chadwick, O.A., L.A. Derry, P.M. Vitousek, B.J. Huebert, and L.O. Hedin. 1999. Changing sources of nutrients during four million years of ecosystem development. *Nature* 397:491–497.

Cowling, S.A. 1999. Plants and temperature: CO_2 uncoupling. *Science* 285:1500–1501.

Demicco, R.V., T.K. Lowenstein, and L.A. Hardie. 2003. Atmospheric pCO_2 since 60 Ma from records of seawater pH, calcium, and primary carbonate mineralogy. *Geology* 31:793–796.

Ekart, D.D., T.E. Cerling, I.P. Montanez, and N.J. Tabor. 1999. A 400 million year carbon isotope record of pedogenic carbonate: implications for paleoatmospheric carbon dioxide. *American Journal of Science* 299:805–827.

FAO. 1988. Soil Map of the World, I: Revised Legend. Rome, UNESCO.

Graham, A. 1999. Late Cretaceous and Cenozoic history of North American vegetation. Oxford University Press, New York. 370 pp.

Hornibrook, N.D.B. 1990. New Zealand Cenozoic marine paleoclimates: a review based on the distribution of some shallow water and terrestrial biota. Pp. 583–606 *in* R. Tsuchi and J. Ingle (eds.). Pacific Neogene Environments, Evolution and Events. University of Tokyo Press, Tokyo.

Itoigawa, J., and T. Yamanoi. 1990. Climatic optimum in the mid-Neogene of the Japanese Islands. Pp. 3–14 *in* R. Tsuchi and J. Ingle (eds.). Pacific Neogene Environments, Evolution and Events. University of Tokyo Press, Tokyo.

Janis, C.M., K.M. Scott, and L.L. Jacobs (eds.). 1998. Evolution of terrestrial mammals of North America, Vol. 1: Terrestrial carnivores, ungulates and ungulatelike mammals. Cambridge University Press, Cambridge. 705 pp.

Kuerschner, W.M., Z. Kvacek, and L.R. Kump. 2002. Palaeoatmospheric CO_2 during the mid-Miocene climate change. *EOS, Transactions, American Geophysical Union* 83(47):F387.

Markewich, H.W., M.J. Pavich, and G.R. Buell. 1990. Contrasting soils and landscapes of the Piedmont and coast plain, eastern United States. *Geomorphology* 3(3–4):417–447.

Maynard, J.B. 1992. Chemistry of modern soils as a guide to interpreting Precambrian paleosols. *Journal of Geology* 100: 279–289.

McGowran, B., and Q. Li. 1997. Miocene climatic oscillation recorded in the Lakes Entrance oil shaft, southern Australia: Reappraisal of the planktonic foraminiferal record. *Micropaleontology* 43:129–148.

Moore, E.J. 1963. Miocene marine mollusks from the Astoria Formation in Oregon. *U.S. Geological Survey Professional Paper* 419, 109 pp.

Mukhopadhyay, P.K. 1992. Maturation of organic matter as revealed by microscopic methods: applications and limitations of vitrinite reflectance, and continuous spectral and pulsed laser fluorescence spectroscopy. Pp. 435–505 *in* K.H.Wolf and G.V. Chilingarian (eds.). Diagenesis, III: *Developments in Sedimentology* 47. Elsevier, New York.

Pagani, M., M.A. Arthur, and K.H. Freeman. 2000. Variations in Miocene phytoplankton growth rates in the southwest Atlantic: evidence for changes in ocean circulation. *Paleoceanography* 15: 486–496.

Pagani, M., K.H. Freeman, and M.A. Arthur. 1999. Late Miocene atmospheric CO_2 concentration and the expansion of C_4 grasses. *Science* 285:876–878.

Pearson, P.N., and M.R. Palmer. 2000. Atmospheric carbon dioxide concentrations over the past 60 million years. *Nature* 406: 695–699.

Palandri, J.L., and M.H. Reed. 2001. Reconstruction of in situ composition of sedimentary formation waters. *Geochimica et Cosmochimica Acta* 65:1741–1767.

Retallack, G.J. 2001a. A 300-million-year record of atmospheric carbon dioxide from fossil plant cuticles. *Nature* 411:287–290.

Retallack, G.J. 2001b. Soils of the Past, 2nd Edition. Blackwell, Oxford. 404 pp.

Retallack, G.J. 2002. Carbon dioxide and climate over the past 300 million years. *Philosophical Transations of the Royal Society of London* 360:659–673.

Retallack, G.J., E.A. Bestland, and T.J. Fremd. 2000. Eocene and Oligocene paleosols of central Oregon. *Geological Society of America Special Paper* 344, 192 pp.

Royer, D.L., S.L. Wing, D.J. Beerling, D.W. Jolley, P.L. Koch, L.J. Hickey, and R.A. Berner. 2001. Paleobotanical evidence for near present-day levels of atmospheric CO_2 during part of the Tertiary. *Science* 292:2310–2313.

Schwarz, T. 1997. Lateritic bauxite in central Germany and implications for Miocene palaeoclimate. *Palaeogeography, Palaeoclimatology, Palaeoecology* 129:37–50.

Sheldon, N.D. 2003. Pedogenesis and geochemical alteration of Columbia River Basalts, Picture Gorge, Oregon. *Geological Society of America Bulletin* 115:1377–1387.

Sheldon, N.D., and G.J. Retallack. 2001. Equation for compaction of paleosols due to burial. *Geology* 29:247–250.

Sheldon, N.D., G.J. Retallack, and S. Tanaka. 2002. Geochemical climofunctions from North American soils and application to paleosols across the Eocene-Oligocene boundary in Oregon. *Journal of Geology* 110:687–696.

Soil Survey Staff. 1975. Soil Taxonomy: A Basic System of Classification for Making and Interpreting Soil Surveys. United States Department of Agriculture Soil Conservation Service, Washington, D.C. 754 pp.

Tanner, L.H., J.F. Hubert, B.P. Coffey, and D.P. McInerney. 2001. Stability of atmospheric CO_2 levels across the Triassic/Jurassic boundary. *Nature* 411:675–677.

Tolan, T.L., S.P. Reidel, M.H. Beeson, J.L. Anderson, K.R. Fecht,

and D.A. Swanson. 1989. Revisions to the estimates of the areal extent and volume of the Columbia River Basalt Group. Pp. 1–20 *in* S.P. Reidel and P.R. Hooper (eds.). Volcanism and Tectonism in the Columbia River Flood-Basalt Province. Geological Society of America Special Paper 239.

Utescher, T., U. Mossbrugger, and A.R. Ashraf. 2000. Terrestrial climate evolution in northwest Germany over the last 25 million years. *Palaios* 15:430–449.

Volk, T. 1987. Feedbacks between weathering and atmospheric CO_2 over the last 100 million years. *American Journal of Science* 287:263–279.

Zachos, J., M. Pagani, L. Sloan, E. Thomas, and K. Billups. 2001. Trends, rhythms, and aberrations in global climate 65 Ma to present. *Science* 292:686–693.